

Screening two-dimensional pyroelectric materials based on pentagonal chains with large shift current

Jiaqi Xin,¹ Yaguang Guo,^{1,*} and Qian Wang²

¹*Department of Physics, School of Physical Science and Engineering, Beijing Jiaotong University, Beijing 100044, China*

²*School of Materials Science and Engineering, Peking University, Beijing 100871, China*



(Received 8 April 2023; revised 19 June 2023; accepted 26 June 2023; published 7 July 2023)

The bulk photovoltaic effect (BPVE) of two-dimensional (2D) polar crystals has received considerable attention in recent years due to its potential applications in high-efficiency energy harvesting. Here, we propose a class of pentagonal chain-based 2D pyroelectric $\text{CuXX}'\text{Y}$ ($X, X' = \text{S, Se, Te}$; $Y = \text{Cl, Br, I}$) monolayers with in-plane polarization via a high-throughput screening method. By using first-principles calculations, we show that compared to the 2D nonpolar CuX_2Y compounds, the alignment between the averaged transition intensity and shift vector of the polar $\text{CuXX}'\text{Y}$ materials gives rise to the enhanced shift current responses reaching up to $500 \mu\text{A V}^{-2}$ in the visible range, and the magnitude of the shift current is positively related to the polarity of the $X\text{-}X'$ bond. More importantly, we find that all the studied materials have their exfoliation energies comparable to those of existing 2D materials, implying the feasibility for preparing $\text{CuXX}'\text{Y}$ monolayers by mechanical exfoliation. Our study demonstrates the potential of utilizing pentagonal chains in the design of polar materials with strong BPVE responses.

DOI: [10.1103/PhysRevMaterials.7.074001](https://doi.org/10.1103/PhysRevMaterials.7.074001)

I. INTRODUCTION

The bulk photovoltaic effect (BPVE) is a nonlinear optical process that can directly convert light into electricity without the need of a built-in electric field at p-n junctions or interfaces to separate the electron-hole pairs. Thus, it can be realized in a single-phase material with a solar cell efficiency higher than the Shockley-Queisser limit [1]. The dominant factor for the BPVE is the shift current that arises from the asymmetric evolution of electron wavefunctions during band transition. For this reason, the BPVE is only present in crystals without inversion symmetry. Polar materials are of great interest in BPVE applications, because the existence of electric polarization naturally satisfies all the requirements for shift current generation. Early studies have shown that the photocurrent collection via BPVE with an efficiency larger than 10% can be achieved in ferroelectric hybrid and oxide perovskites [2,3], which has motivated considerable research on ferroelectric photovoltaics. As a result, many 2D ferroelectric crystals, such as group IV monochalcogenides [4,5], $\alpha\text{-In}_2\text{Se}_3$ [6], and selenium and tellurium monolayers [7], have been recently predicted for promising BPVE materials. Especially, a strong BPVE has been experimentally observed in 2D hybrid perovskites [8] and CuInP_2S_6 [9], which opened up a new way for developing novel solar cells by using ultrathin ferroelectric sheets.

Besides ferroelectrics, 2D structures with electric polarization can also be artificially designed. For instance, recent experimental studies based on symmetry engineering have been conducted to induce polarization in transition-metal

dichalcogenides for large shift current generation by rolling bilayer WS_2 into a polar nanotube [10], stacking WSe_2 and black phosphorene to form a polar interface [11], or applying a strain gradient on MoS_2 to obtain a polar monolayer (flexophotovoltaic effect) [12]. Theoretically, Schankler *et al.* [13] found an enhanced BPVE in MoS_2 by inducing polarization via an electric field, which is called a bulk piezophotovoltaic effect.

These studies highlight the importance of electric polarization for enhancing shift current, while the real application is hindered by the complicated setup for symmetry reduction in such nonpolar structures. In this regard, 2D pyroelectric materials are promising alternatives due to their intrinsic polar symmetry. Moreover, unlike ferroelectrics that become paraelectric with a phase transition above the Curie temperature, the electric polarization in pyroelectrics is a structural property independent of temperature, thus enabling the application at elevated temperatures. In recent years, Janus structuring has been widely used to design 2D pyroelectric crystals with asymmetric surfaces (called Janus materials) [14,15], which led to the emergence of out-of-plane dipole moments and a superior BPVE response [16]. However, the rational design of in-plane polar symmetry in 2D materials and the consequent nonlinear optical properties remain largely unexplored.

Here, we propose a new strategy to screen 2D pyroelectric materials based on pentagonal chains, and find a class of 2D quaternary $\text{CuXX}'\text{Y}$ ($X, X' = \text{S, Se, Te}$; $Y = \text{Cl, Br, I}$) compounds with in-plane polarization as well as large shift currents ($\sim 500 \mu\text{A V}^{-2}$). Although a larger polarization does not always ensure a stronger BPVE response, we do find that the shift current and electric polarization in our studied systems have a positive correlation. Moreover, compared with the nonpolar CuX_2Y sheets, we show that the shift vector

*ygguo@bjtu.edu.cn

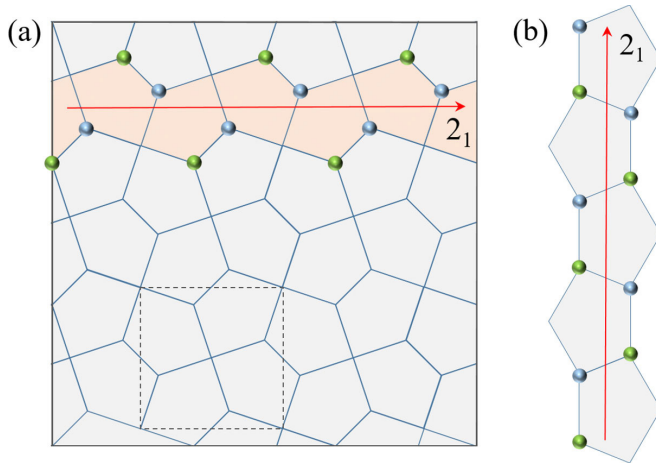


FIG. 1. (a) Cairo pentagonal tiling. The dashed lines represent a unit cell. The orange shaded region shows a polar chain structure with two different atoms on the three-coordinated vertices. The red arrow denotes the twofold screw axis as well as the polarization direction. (b) The pentagonal chain structure with polarization along the chain direction induced by nonequivalent three-coordinated atoms.

distributed near uniformly in the Brillouin zone aligns with the transition intensity at the same photon energy after integration, leading to an enhanced BPVE in these polar $\text{CuXX}'\text{Y}$ monolayers.

II. METHODS

Our first-principles calculations were carried out based on density function theory. We used the Vienna ab Initio Simulation Package [17] with the projector augmented wave method [18]. The electronic exchange-correlation interaction is treated with the Perdew-Burke-Ernzerhof functional within the generalized gradient approximation [19]. The energy cut-off for the plane-wave basis is set to be 500 eV. The density of the Monkhorst-Pack k -point mesh [20] used is $2\pi \times 0.01 \text{ \AA}^{-1}$. All the structures are fully optimized with a convergence threshold of 0.01 eV \AA^{-1} for force and $1 \times 10^{-4} \text{ eV}$ for energy. A vacuum space of 20 \AA is applied in the nonperiodic direction to avoid the interaction between two adjacent layers. The k -point sampling for the shift current tensor calculation is carefully tested (see Supplemental Material Fig. S1 [21]), where a $70 \times 70 \times 1$ grid is used to perform the simulation. Both the DFT-D3 and optB88-vdW methods are used for the van der Waals (vdW) correction.

III. RESULTS AND DISCUSSION

Pentagons are much less common as the building blocks of 2D materials. Compare with hexagons, pentagons naturally have a lower symmetry, which benefits the design of polar materials. Among all the possible 2D pentagon-based configurations [22], Cairo pentagonal tiling is a popular structure model [Fig. 1(a)]. Plenty of 2D materials have been recently predicted and fabricated based on this tiling pattern [23], such as penta-graphene [24], penta-PdSe₂ [25], and penta-NiN₂ [26]. In our previous studies, a strategy was proposed to

realize in-plane spontaneous polarization in such a pentagonal model [27,28], where the polar vector is along the twofold screw axis. This polar symmetry requires two different atoms at neighboring three-coordinated vertices forming polar bonds [green and blue balls in Fig. 1(a)]. Note that the screw axis is located at the middle of the shaded region, which shows a chain-like shape. Interestingly, we notice that the other pentagonal chain structure [Fig. 1(b)] can be obtained based on the configuration of the silicon pentagonal nanoribbons experimentally deposited on the silver (110) surface [29–31]. Although pentagons are arranged differently in these two one-dimensional configurations, the twofold screw axis remains in both cases. Therefore, when neighboring three-coordinated atoms are nonequivalent, a polar chain forms [Fig. 1(b)] that can be utilized to assemble 2D pyroelectric materials.

Here, we demonstrate a high-throughput screening method to identify the 2D polar materials composed of the previously mentioned pentagonal chains based on the Computational 2D Materials Database (C2DB) [32], which is an online repository of crystallographic data and elementary physical properties for more than 4000 2D crystals. As shown in Fig. 1(b), the two neighboring “left-right” connected pentagons are the minimum repeating unit for the chain structure, implying that a single cell of the target material should contain at least one such motif. Thus, our algorithm is designed to determine whether the materials in the database meet this requirement via the following steps, as illustrated in Fig. 2(a): (i) use a 2×2 supercell to ensure that the repeating unit is completely inside the structure for screening (note that two red balls in the pentagons are out of the unit cell); (ii) find all chemical bonds in this supercell, where a bond exists when the atomic distance is less than the sum of their covalent radii; (iii) project all atoms and bonds onto the basal plane (eliminating structural buckling), and calculate all bond angles for the projected structure forming a data set; and (iv) make a summation of ten bond angles selected in the set and iterate over all combinations. If there exists a combination with a summation of 1080° (the interior angle of two pentagons), and the ten bond angles in this combination are made up of eight atoms (blue balls), which exactly form nine chemical bonds (pink lines), the material is identified with pentagonal chains. By applying this protocol to C2DB, we find 13 target materials that have a similar structural motif with a general formula of MX_2Y ($M = \text{Cu, Ag, Au}$; $X = \text{O, S, Se, Te}$; $Y = \text{Cl, Br, I}$), as listed in Supplemental Material Table SI [21]. Among them, four copper-based materials—namely, CuSe_2Cl , CuTe_2Cl , CuTe_2Br , and CuTe_2I —are selected for further study as they have corresponding vdW bulk phases matching the experimentally observed crystals in the Materials Project (MP) database [33]. The screened configuration is plotted in Fig. 2(b), where each pentagon consists of one copper and four X atoms and the pentagonal chains are connected by the bridging Y atoms. The buckled structure breaks the inversion symmetry, however, and the identical three-coordinated atoms cannot induce electric polarization. Thus, the 2D MX_2Y structure is noncentrosymmetric but nonpolar. In order to realize polar systems, we make an isoelectronic substitution by replacing one X atom with a same-group other atom

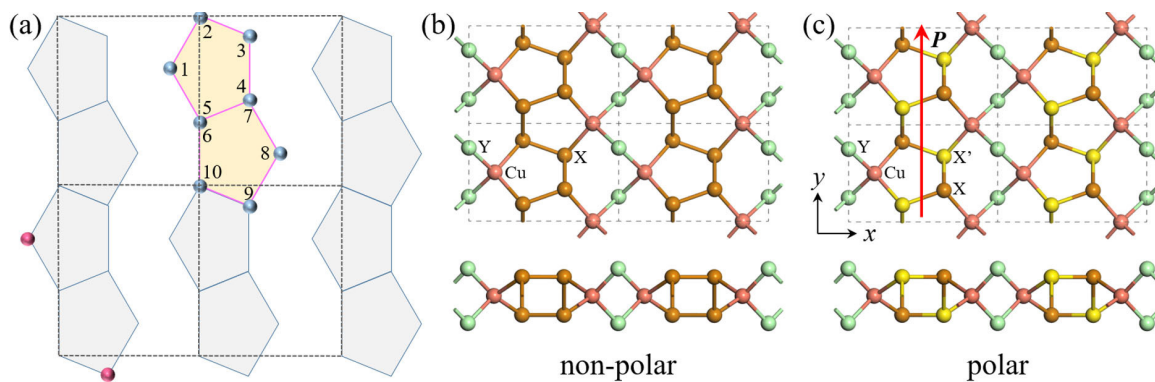


FIG. 2. (a) Schematic of the pentagonal chain configuration in 2D materials. (b) Geometric structure of the nonpolar CuX_2Y sheet composed of CuX_4 pentagonal chains and halogen atoms (Y) as the linker. (c) Geometric structure of the polar $\text{CuXX}'\text{Y}$ sheet composed of $\text{CuX}_2\text{X}'_2$ pentagonal chains and halogen atoms.

X' [Fig. 2(c)]. Consequently, the polar bonds are formed and orderly arranged along the chain direction, exhibiting pyroelectric polarization in the newly quaternary $\text{CuXX}'\text{Y}$ monolayer. We list all the constructed 2D $\text{CuXX}'\text{Y}$ in Supplemental Material Table SII [21] and highlight five structures (CuTeSbCl , CuTeSeCl , CuTeSbBr , CuTeSeBr , and CuTeSeI) that also have their vdW bulk counterparts in the MP database.

Next, we take CuTeSbBr as an example to investigate the BPVE in these polar $\text{CuXX}'\text{Y}$ monolayers. The shift current tensor is given as

$$\sigma^{abc}(0; \omega, -\omega) = -\frac{i\pi e^3}{2\hbar^2} \int [d\mathbf{k}] \sum_{nm} f_{nm} \times (r_{nm}^b r_{nm,a}^c + r_{nm}^c r_{nm,a}^b) \delta(\omega_{mn} - \omega), \quad (1)$$

where a, b, c are Cartesian indices, n and m are the band indices, $f_{nm} = f_n - f_m$ is the Fermi-Dirac occupation number, and $\hbar\omega_{nm} = E_m - E_n$ is the band energy difference. The integral is over the first Brillouin zone with $[d\mathbf{k}] = d\mathbf{k}^d / (2\pi)^d$ in d dimensions, and k is the crystal momentum. r_{nm}^a is the dipole matrix element, which is given by $r_{nm}^a = (1 - \delta_{nm}) A_{nm}^a$, and $r_{nm,b}^a$ represents generalized derivatives with the definition of $r_{nm,b}^a = \partial r_{nm}^a / \partial k^b - i(A_{nm}^b - A_{nm}^a) r_{nm}^a$, where A_{nm}^a is the Berry connection. For 2D systems, the shift current needs to be multiplied by $d_z / d_{\text{thickness}}$ with d_z as the lattice length perpendicular to the periodic direction, and $d_{\text{thickness}}$ as the actual thickness of the monolayer. This transformation is for quantitative comparison with bulk systems. For a more efficient calculation, we employ the Wannier interpolated model proposed by Ibañez-Azpiroz *et al.* [34], where `pyw90` and `WANNIER90` [35] codes are used to obtain the Wannier functions (see Supplemental Material Fig. S2 for details [21]). The largest photoresponse direction of CuTeSbBr is in the polar chain direction, i.e., σ^{yxx} , as plotted in Fig. 3(a). Compared to the nonpolar CuTe_2Br , the maximum peak is increased threefold and can reach $-479 \mu\text{A V}^{-2}$. The integrated shift current in the visible range (1 to 3 eV) is increased even more, because the negative and positive parts in the shift current curve of CuTe_2Br are largely canceled, while the curve for CuTeSbBr keeps almost the same sign. Similar BPVE properties have been found in other screened polar monolayers.

The maximum peaks of CuTeSbCl , CuTeSeCl , CuTeSeBr , and CuTeSeI are $-508 \mu\text{A V}^{-2}$ at $\hbar\omega = 1.88 \text{ eV}$, $-109 \mu\text{A V}^{-2}$ at $\hbar\omega = 1.72 \text{ eV}$, $-134 \mu\text{A V}^{-2}$ at $\hbar\omega = 1.75 \text{ eV}$, and $-87 \mu\text{A V}^{-2}$ at $\hbar\omega = 1.65 \text{ eV}$, respectively (see Supplemental Material Fig. S3 [21]). Such values are larger than those of prototypical ferroelectric oxides, e.g., $5 \mu\text{A V}^{-2}$ in BaTiO_3 [3], and many other emerging materials such as 2D ferroelectrics [4] and Weyl semimetals [36] within the same photon energy range. Thus, the BPVE for 2D $\text{CuXX}'\text{Y}$ is strong for optoelectronic applications. Note that the effect of spin-orbit coupling on the shift current is also considered, which does not lead

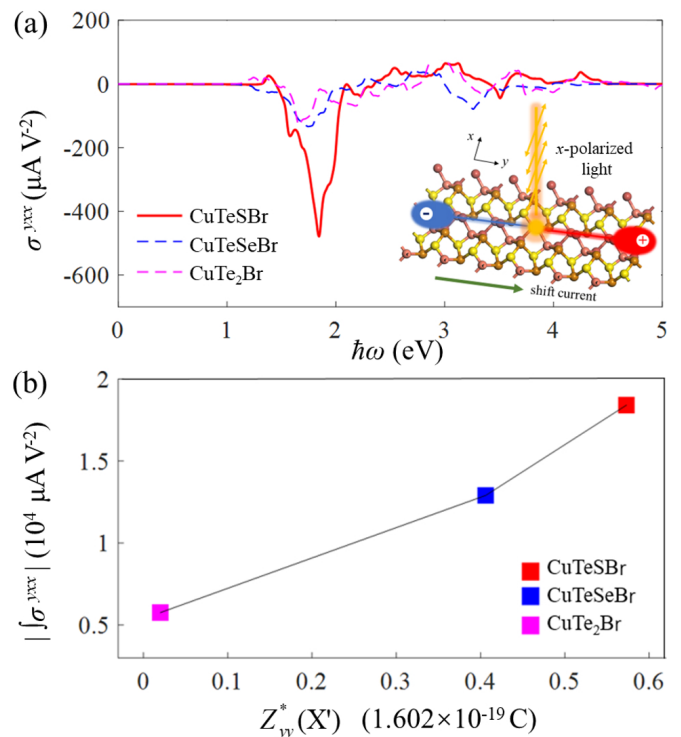


FIG. 3. (a) Shift current tensor σ^{yxx} of CuTeSbBr , CuTeSeBr , and CuTe_2Br . The inset image illustrates the direction of σ^{yxx} with respect to the orientation of the electric field and polarization axis. (b) The relationship between the integrated shift current and the Born effective charge $Z_{yy}^*(X')$.

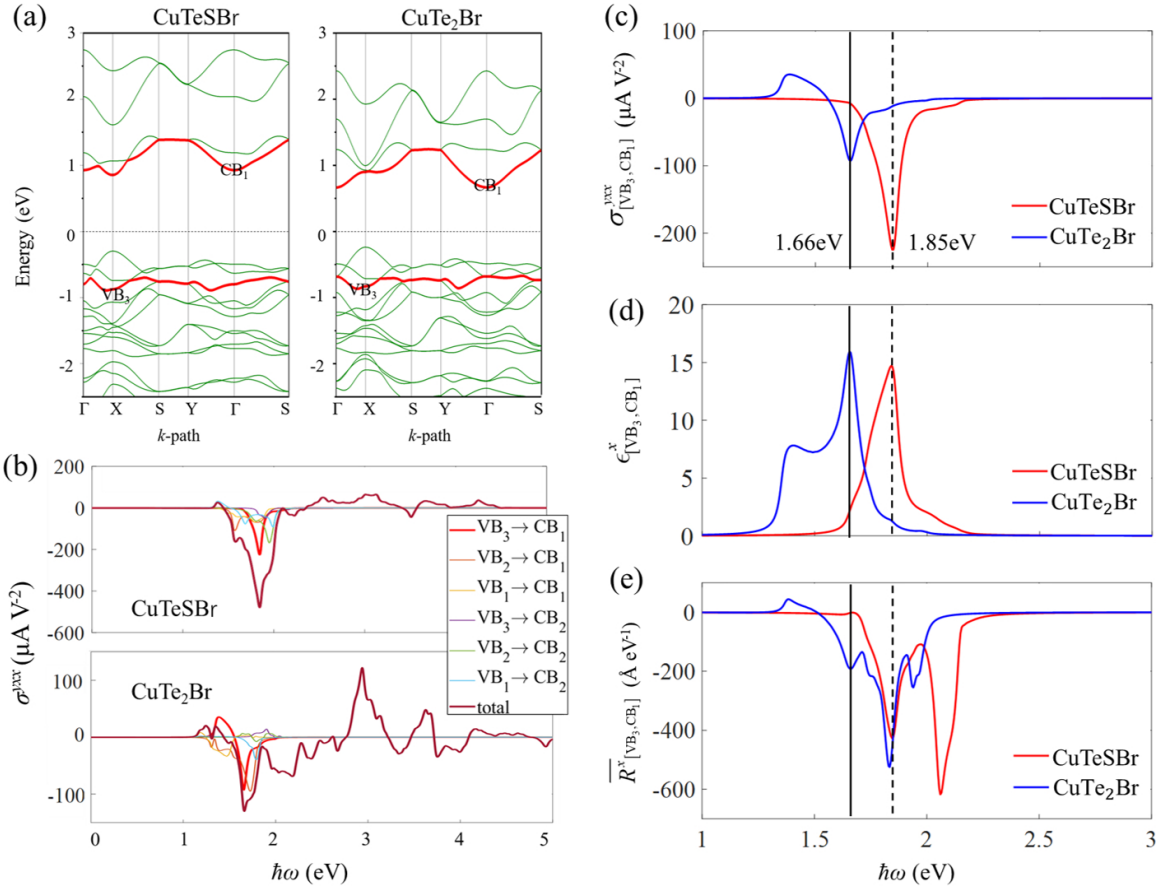


FIG. 4. (a) Band structures of the CuTeSBr and CuTe₂Br sheets. The red bands contribute most to the peak value of the shift current. (b) The shift current response between different band pairs. The red line for VB₃ → CB₁ represents the largest contribution. The (c) shift current, (d) transition intensity, and (e) aggregate shift vector contributed from the (VB₃ → CB₁) pair.

to significant changes (see Supplemental Material Figs. S4 and S5 [21]).

It is worth mentioning that the shift current and electric polarization are not correlated in a specific way, especially in complex materials [3,37]. However, many studies have pointed out that a polar crystal structure is crucial for enhancing BPVE [9–11]. In periodic systems, the absolute value of polarization is multivalued [38]. Here, we calculate the yy component of the Born effective charge tensor for the X' atom, i.e., $Z_{yy}^*(X')$, to measure the magnitude of polarization in CuXX'Br monolayers. Figure 3(b) clearly shows that $Z_{yy}^*(X')$ has a positive relationship with the integral of the shift current tensor over the frequency range (up to 5 eV), i.e., $|\int \sigma^{yxx}|$. The same trend is also found in the other 2D CuXX'Y materials (see Supplemental Material Fig. S6 for details [21]). Therefore, inducing polarization in nonpolar CuX₂Y systems is a possible strategy to design BPVE materials with tailored nonlinear optical responses.

To understand the microscopic mechanism for the enhanced BPVE in such polar systems, we split the shift current tensor into two components of the shift vector and transition intensity. The shift vector R_{nm}^b is defined as $R_{nm}^b = \partial \phi_{nm}(k) / \partial k^b - A_{mm}^b + A_{nn}^b$ with ϕ_{nm} as the phase of $r_{nm}^b = |r_{nm}^b| e^{-i\phi_{nm}}$. It has the unit of length, describing the average displacement from band m to band n during the lifetime of an electron after absorbing a photon. Over the

same period of time, the longer the carriers travel, the stronger the shift current response is excited. The shift vector can be calculated with $R_{nm}^b = \text{Im}[r_{mn}^b r_{nm;a}^b + r_{mn}^b r_{nm;a}^b] / |r_{nm}^b|^2$. As an analytical tool, we integrate R_{nm}^b over the Brillouin zone between band m to band n :

$$\overline{R}_{[n,m]}^b(\omega) = \int [dk] f_{nm} R_{nm}^b \delta(\omega_{nm} - \omega). \quad (2)$$

Note that $\overline{R}_{[n,m]}^b$ is not physical, but it can be used to plot the aggregate shift vector curve under different light energy for qualitative analysis. When separating R_{nm}^b from Eq. (1), there leaves a term of $|r_{nm}^b|^2$, which is proportional to the transition intensity from band m to band n , written as

$$\varepsilon_{[n,m]}^b(\omega) = \frac{i\pi e^2}{\hbar} \int [dk] f_{nm} |r_{nm}^b|^2 \delta(\omega_{nm} - \omega). \quad (3)$$

In terms of Eqs. (2) and (3), the shift current responses contributed from different band pairs are first examined as shown in Figs. 4(a) and 4(b), where we find that the largest contribution to the main peak for both polar CuTeSBr (1.85 eV) and nonpolar CuTe₂Br (1.66 eV) is from the transition between the third highest valence band (denoted VB₃) and the lowest conduction band (denoted CB₁). This is because the transition matrix element and joint density of states are largely overlapped for this band pair in the Brillouin

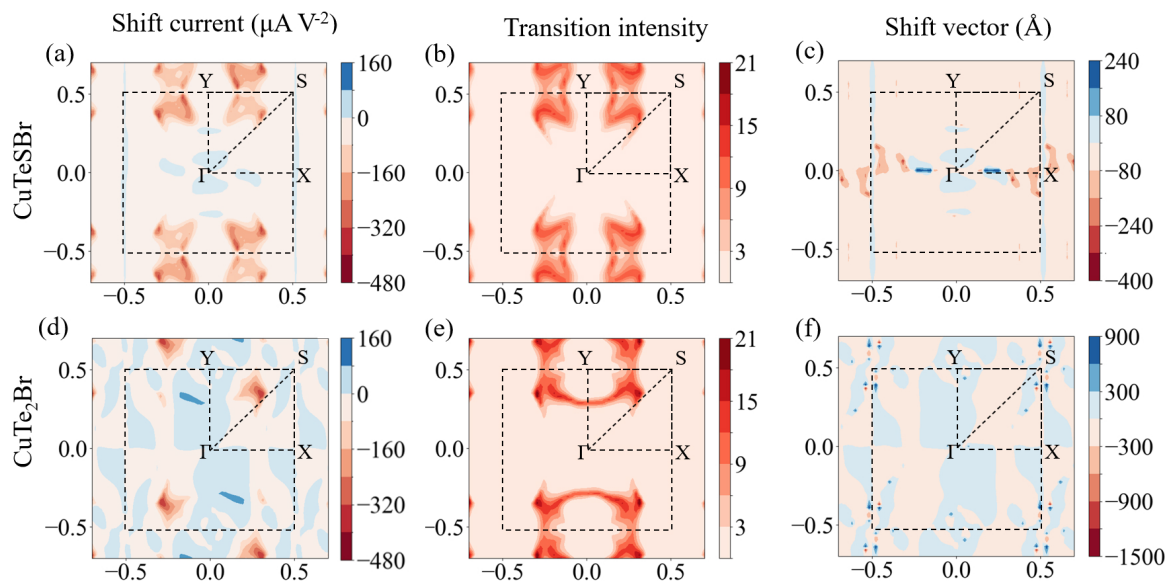


FIG. 5. The k -resolved (a) shift current, (b) transition intensity, and (c) shift vector between VB_3 and CB_1 of CuTeSBr at $\hbar\omega = 1.85$ eV. (d)–(f) The same physical quantities of CuTe₂Br at $\hbar\omega = 1.66$ eV.

zone (see Supplemental Material Figs. S7–S9 for the details [21]). Based on this, we calculate the shift current, transition intensity, and aggregate shift vector for the ($VB_3 \rightarrow CB_1$) pair as plotted in Figs. 4(c)–4(e). The maximum values of $\varepsilon_{[VB_3, CB_1]}^x(\omega)$ in CuTeSBr and CuTe₂Br are close [Fig. 4(d)], and their peak positions are consistent with those of $\sigma_{[VB_3, CB_1]}^{yxx}$ [Fig. 4(c)]. Therefore, $\bar{R}_{[VB_3, CB_1]}^x$ dominates the magnitude of shift current response. In Fig. 4(e), one can see that the $\bar{R}_{[VB_3, CB_1]}^x$ for CuTeSBr at 1.85 eV is nearly three times as large as that for CuTe₂Br at 1.66 eV, hence giving rise to the BPVE enhancement in polar structure.

According to Eq. (1), the point with the large transition intensity and shift vector in the Brillouin zone can lead to a strong BPVE response; thus, we further plot k -resolved values in Fig. 5 to understand the previous aggregate quantities. The transition intensities of both materials share a similar distribution [Figs. 5(b) and 5(e)]. However, the dipole transition is forbidden around the middle point of the $\Gamma \rightarrow Y$ line in polar CuTeSBr due to the changed band symmetry. This explains the slightly larger peak of transition intensity in CuTe₂Br than that in CuTeSBr. Moreover, because the transition intensity is always positive ($\propto |r_{mm}^b|^2$), the sign of the shift current is consistent with that of the shift vector. Both strong positive and negative values of the shift vector are observed in CuTe₂Br [Fig. 5(f)]; thus, the cancellation between them reduces the net current after integration over the Brillouin zone [Fig. 5(d)]. In contrast, the shift current contains most features of the transition intensity in CuTeSBr [Figs. 5(a) and 5(b)], since the shift vector is nearly negative in the whole Brillouin zone, although its absolute value decreases [Fig. 5(c)]. Such a pattern of distribution avoids strong cancellation, consequently leading to the enhanced shift current. As discussed elsewhere [13], the shift vector is a decisive factor for determining the BPVE response, which can be modulated significantly by changing the crystal configuration, such as inducing atomic displacement.

Here, we show that isoelectronic atom substitution is another effective approach to realizing a strong shift current.

To examine the feasibility of fabricating these pyroelectric CuXX'Y monolayers from their vdW bulk counterparts, we calculate the exfoliation energies, defined as the energy cost for stripping the top layer from the surface of the bulk crystal [39], written as

$$E_{\text{exf}} = \frac{E_{\text{iso}} - E_{\text{bulk}}/N}{S}, \quad (4)$$

where E_{iso} is the energy of the isolated CuXX'Y monolayer, E_{bulk}/N is the energy of the corresponding bulk structure per layer, and S is the in-plane area of the bulk unit cell. We find that the values of E_{exf} are in the range of 21.22 to 24.28 meV/Å² [see Table I], which are comparable to those of graphene, hexagonal-BN, and phosphorene [39], indicating that these 2D CuXX'Y materials could be synthesized by mechanical exfoliation from bulk phases. In addition, the stabilities of freestanding CuXX'Y sheets are further examined by calculating their phonon spectra, as plotted in Supplemental Material Fig. S10 [21], where no imaginary frequencies exist throughout the entire Brillouin zone, indicating that these polar monolayers are dynamically stable. We also list the energy above hull of CuXX'Y bulk structures in Supplemental

TABLE I. Exfoliation energies for CuXX'Y monolayers with different vdW corrections.

meV/Å ²	DFT-D3	optB88-vdW
CuTeSBr	23.03	22.53
CuTeSCl	23.27	22.32
CuTeSeBr	21.22	22.72
CuTeSeCl	24.28	22.32
CuTeSeI	24.11	23.00

Material Table SII [21]. The values are in the range of 50 to 100 meV; thus, these materials are considered to be thermodynamically metastable.

IV. CONCLUSION

In summary, we have proposed a new class of 2D pyroelectric materials $\text{CuXX}'\text{Y}$ ($X, X' = \text{S, Se, Te}$; $Y = \text{Cl, Br, I}$) containing pentagonal chains by using a high-throughput screening method. Compared to the nonpolar CuX_2Y monolayers, the identified polar monolayers exhibit stronger shift current responses (up to $500 \mu\text{A V}^{-2}$) that are positively correlated to electric polarization. The enhancement of the BPVE is due to the nearly uniform distribution of the shift vector in the Brillouin zone, which suppresses the strong cancellation in shift current integration. Moreover, the calculated exfoliation energies show the feasibility of mechanically exfoliating

these polar $\text{CuXX}'\text{Y}$ sheets from their bulk counterparts. These results not only suggest that 2D $\text{CuXX}'\text{Y}$ sheets are novel BPVE materials, but also show the advantages of using pentagonal chains as the building units in the design of polar materials, expanding the family of 2D pyroelectric materials and unlocking their potential applications in photovoltaics.

ACKNOWLEDGMENT

The authors thank Professor Jian Zhou for his helpful discussion. This work is supported by grants from the Fundamental Research Funds for the Central Universities (Grant No. 2021JBM041) and the National Natural Science Foundation of China (Grant No. 12104037). It is also supported by the High-Performance Computing Platform of Beijing Jiaotong University, China.

-
- [1] W. Shockley and H. J. Queisser, *J. Appl. Phys.* **32**, 510 (1961).
- [2] S. Y. Yang, J. Seidel, S. J. Byrnes, P. Shafer, C.-H. Yang, M. D. Rossell, P. Yu, Y.-H. Chu., J. F. Scott Chu, J. W. Ager III, L. W. Martin, and R. Ramesh, *Nat. Nanotechnol.* **5**, 143 (2010).
- [3] S. M. Young and A. M. Rappe, *Phys. Rev. Lett.* **109**, 116601 (2012).
- [4] T. Rangel, B. M. Fregoso, B. S. Mendoza, T. Morimoto, J. E. Moore, and J. B. Neaton, *Phys. Rev. Lett.* **119**, 067402 (2017).
- [5] S.-J. Gong, F. Zheng, and A. M. Rappe, *Phys. Rev. Lett.* **121**, 017402 (2018).
- [6] R. P. Tiwari, B. Birajdar, and R. K. Ghosh, *Phys. Rev. B* **101**, 235448 (2020).
- [7] M. Cheng, Z.-Z. Zhu, and G.-Y. Guo, *Phys. Rev. B* **103**, 245415 (2021).
- [8] P.-J. Huang, K. Taniguchi, and H. Miyasaka, *Chem. Mater.* **34**, 4428 (2022).
- [9] Y. Li, J. Fu, X. Mao, C. Chen, H. Liu, M. Gong, and H. Zeng, *Nat. Commun.* **12**, 5896 (2021).
- [10] Y. Zhang, T. Ideue, M. Onga, F. Qin, R. Suzuki, A. Zak, R. Tenne, J. Smet, and Y. Iwasa, *Nature (London)* **570**, 349 (2019).
- [11] T. Akamatsu, T. Ideue, L. Zhou, Y. Dong, S. Kitamura, M. Yoshii, D. Yang, M. Onga, Y. Nakagawa, K. Watanabe, T. Taniguchi, J. Lauritzen, J. Huang, Z. Ye, T. Morimoto, H. Yuan, and Y. Iwasa, *Science* **372**, 68 (2021).
- [12] J. Jiang, Z. Chen, Y. Hu, Y. Xiang, L. Zhang, Y. Wang, G.-C. Wang, and J. Shi, *Nat. Nanotechnol.* **16**, 894 (2021).
- [13] A. M. Schankler, L. Gao, and A. M. Rappe, *J. Phys. Chem. Lett.* **12**, 1244 (2021).
- [14] J. Zhang, S. Jia, I. Kholmanov, L. Dong, D. Er, W. Chen, H. Guo, Z. Jin, V. B. Shenoy, L. Shi, and J. Lou, *ACS Nano* **11**, 8192 (2017).
- [15] A.-Y. Lu, H. Zhu, J. Xiao, C.-P. Chuu, Y. Han, M.-H. Chiu, C.-C. Cheng, C.-W. Yang, K.-H. Wei, Y. Yang, Y. Wang, D. Sokaras, D. Nordlund, P. Yang, D. A. Muller, M.-Y. Chou, X. Zhang, and L.-J. Li, *Nat. Nanotechnol.* **12**, 744 (2017).
- [16] A. Strasser, H. Wang, and X. Qian, *Nano Lett.* **22**, 4145 (2022).
- [17] G. Kresse and J. Furthmüller, *Phys. Rev. B* **54**, 11169 (1996).
- [18] P. E. Blöchl, *Phys. Rev. B* **50**, 17953 (1994).
- [19] J. P. Perdew, K. Burke, and M. Ernzerhof, *Phys. Rev. Lett.* **77**, 3865 (1996).
- [20] H. J. Monkhorst and J. D. Pack, *Phys. Rev. B* **13**, 5188 (1976).
- [21] See Supplemental Material at <http://link.aps.org/supplemental/10.1103/PhysRevMaterials.7.074001> for structural information of all the studied 2D materials. In addition, supplemental figures are plotted for their electronic, optical, and vibrational properties as well as a k -mesh convergence test of the BPVE response.
- [22] Y. Shen and Q. Wang, *Phys. Rep.* **964**, 1 (2022).
- [23] M. A. Nazir, A. Hassan, Y. Shen, and Q. Wang, *Nano Today* **44**, 101501 (2022).
- [24] S. Zhang, J. Zhou, Q. Wang, X. Chen, Y. Kawazoe, and P. Jena, *Proc. Natl. Acad. Sci. USA* **112**, 2372 (2015).
- [25] A. D. Oyedele, S. Yang, L. Liang, A. A. Puzos, K. Wang, J. Zhang, P. Yu, P. R. Pudasaini, A. W. Ghosh, Z. Liu, C. M. Rouleau, B. G. Sumpter, M. F. Chisholm, W. Zhou, P. D. Rack, D. B. Geohegan, and K. Xiao, *J. Am. Chem. Soc.* **139**, 14090 (2017).
- [26] M. Bykov, E. Bykova, A. V. Ponomareva, F. Tasnádi, S. Chariton, V. B. Prakapenka, K. Glazyrin, J. S. Smith, M. F. Mahmood, I. A. Abrikosov, and A. F. Goncharov, *ACS Nano* **15**, 13539 (2021).
- [27] Y. Guo, C. Zhang, J. Zhou, Q. Wang, and P. Jena, *Phys. Rev. Appl.* **11**, 064063 (2019).
- [28] Y. Guo, J. Zhou, H. Xie, Y. Chen, and Q. Wang, *npj Comput. Mater.* **8**, 40 (2022).
- [29] G. Prévot, C. Hogan, T. Leoni, R. Bernard, E. Moyen, and L. Masson, *Phys. Rev. Lett.* **117**, 276102 (2016).
- [30] J. I. Cerdá, J. Sławińska, G. Le Lay, A. C. Marele, J. M. Gómez-Rodríguez, and M. E. Dávila, *Nat. Commun.* **7**, 13076 (2016).
- [31] S. Sheng, R. Ma, J.-B. Wu, W. Li, L. Kong, X. Cong, D. Cao, W. Hu, J. Gou, J.-W. Luo, P. Cheng, P.-H. Tan, Y. Jiang, L. Chen, and K. Wu, *Nano Lett.* **18**, 2937 (2018).
- [32] M. N. Gjerding, A. Taghizadeh, A. Rasmussen, S. Ali, F. Bertoldo, T. Deilmann, N. R. Knøsgaard, M. Kruse, A. H. Larsen, S. Manti, T. G. Pedersen, U. Petralanda, T. Skovhus, M. K. Svendsen, J. J. Mortensen, T. Olsen, and K. Sommer Thygesen, *2D Mater.* **8**, 044002 (2021).

- [33] A. Jain, S. P. Ong, G. Hautier, W. Chen, W. D. Richards, S. Dacek, S. Cholia, D. Gunter, D. Skinner, G. Ceder, and K. A. Persson, *APL Mater.* **1**, 011002 (2013).
- [34] J. Ibañez-Azpiroz, S. S. Tsirkin, and I. Souza, *Phys. Rev. B* **97**, 245143 (2018).
- [35] A. A. Mostofi, J. R. Yates, G. Pizzi, Y.- S. Lee, I. Souza, D. Vanderbilt, and N. Marzari, *Comput. Phys. Commun.* **185**, 2309 (2014).
- [36] G. B. Osterhoudt, L. K. Diebel, M. J. Gray, X. Yang, J. Stanco, X. Huang, B. Shen, N. Ni, P. J. W. Moll, Y. Ran, and K. S. Burch, *Nat. Mater.* **18**, 471 (2019).
- [37] L. Z. Tan, F. Zheng, S. M. Young, F. Wang, S. Liu, and A. M. Rappe, *npj Comput. Mater.* **2**, 1 (2016).
- [38] N. A. Spaldin, *J. Solid State Chem.* **195**, 2 (2012).
- [39] J. H. Jung, C.-H. Park, and J. Ihm, *Nano Lett.* **18**, 2759 (2018).